

IPA in the Loop: Control Design for Throughput Regulation in Computer Processors

X. Chen, Y. Wardi, and S. Yalamanchili

Abstract—A new technique for performance regulation in event-driven systems, recently proposed by the authors, consists of an adaptive-gain integral control. The gain is adjusted in the control loop by a real-time estimation of the derivative of the plant-function with respect to the control input. This estimation is carried out by Infinitesimal Perturbation Analysis (IPA). The main motivation comes from applications to throughput regulation in computer processors, where to-date, testing and assessment of the proposed control technique has been assessed by simulation. The purpose of this paper is to report on its implementation on a machine, namely an Intel Haswell microprocessor, and compare its performance to that obtained from cycle-level, full system simulation environment. The intrinsic contribution of the paper to the Workshop on Discrete Event System is in describing the process of taking an IPA-based design and simulation to a concrete implementation, thereby providing a bridge between theory and applications.

I. INTRODUCTION

One of the objectives of systems' control is *performance regulation*, namely the output tracking of a given setpoint reference despite modeling uncertainties, time-varying system's characteristics, noise, and other unpredictable factors having the effects of system-disturbances. A commonly-practiced way to achieve tracking is by a feedback control law that includes an integrator. An integral control alone may have destabilizing effects on the closed-loop system, and hence the controller often includes proportional and derivative elements as well thereby comprising the well-known PID control [1].

Recently there has been a growing interest in performance regulation of event-driven systems, including Discrete Event Dynamic Systems (DEDS) and Hybrid Systems (HS), and a control technique has been proposed which leverages on the special structure of discrete-event dynamics [2]. The controller consists of a standalone integrator with an adaptive gain, adjusted in real time as part of the control law. The rule for changing the gain is designed for stabilizing the closed-loop system as well as for simplicity of implementation and robustness to computational and measurement errors. Therefore it obviates the need for proportional and derivative elements, and can be implemented in real-time environments by approximating complicated computations by simpler ones. In other words, the balance between precision and required computing efforts can be tilted in favor of simple, possibly imprecise computations. A key feature of the control law is that it is based on the derivative of the plant function, namely

the relation between the system's control parameter and its output, which is computed or estimated by Infinitesimal Perturbation Analysis (IPA). This will be explained in detail in the following paragraphs.

IPA is a well-known and well-tested technique for computing sample-performance derivatives (gradients) in DEDS, HS, and other event-driven systems with respect to controlled variables; see [3], [4] for extensive presentations and surveys. Its salient feature is in simple rules for tracking the propagations associated with a gradient along the sample path of a system, by low-cost algorithms. However, this simplicity may come at the expense of statistical unbiasedness of the IPA derivatives. In situations where IPA is biased, alternative perturbation-analysis techniques have been proposed, but they may require far-larger computing efforts than the basic IPA (see [3], [4]). For the performance regulation technique described in this paper, it has been shown that IPA need not be unbiased and, as mentioned earlier, its most important requirement is low computational complexity [2].

The control system we consider is depicted in Figure 1. Assuming discrete time and one-dimensional variables, r is the setpoint reference, $n = 0, 1, \dots$ denotes the time counter, the control variable u_n is the input to the plant at time n , y_n is the corresponding output, and $e_n := r - y_n$ is the error signal at time n . The control law is defined by the following equation,

$$u_n = u_{n-1} + A_n e_{n-1}, \quad (1)$$

and we recognize this as an adder, the discrete-time analogue of an integrator, if the gain A_n is a constant that does not depend on n . The plant is an event-driven dynamical system whose output y_n is related to its input u_n in a manner defined in the next paragraph, and denoted by the functional term

$$y_n = L_n(u_n), \quad (2)$$

where $L_n : R \rightarrow R$ is a random function. Its IPA derivative $L'_n(u_n) := \frac{\partial y_n}{\partial u_n}$ is used to define the controller's gain A_{n+1} via the equation

$$A_{n+1} = \left(L'_n(u_n) \right)^{-1}, \quad (3)$$

and the error signal is defined as

$$e_n = r - y_n. \quad (4)$$

A recursive application of Eqs. (1)-(4) defines the closed-loop system.

As for the plant, it can have the following form. Consider a continuous-time or discrete-time dynamical system whose input is $u(t) \in R$, and its state is $z(t) \in R^q$ for some $q \geq 1$; the

Research supported in part by the NSF under Grant Number CNS-1239225.

School of Electrical and Computer Engineering, Georgia Institute of Technology, Atlanta, GA 30332, USA. Email: xchen318@gatech.edu, ywardi@ece.gatech.edu, sudha@ece.gatech.edu.

notation t designates continuous time or discrete time. Let $g : R^q \rightarrow R$ be a function that is absolutely integrable over finite-length intervals. Partition the time-axis $\{t \geq 0\}$ into contiguous left-closed, right-open intervals, C_1, C_2, \dots , called *control cycles*. Suppose that the input to the latter dynamical system has constant values during each interval C_n , and it can be changed only at the boundary of these intervals. In the setting of the system of Figure 1, u_n is the value of the input $u(t)$ during C_n , and y_n can be either $y_n := \int_{C_n} g(z(t))dt$ or $y_n := \int_{C_n} g(z(t))dt/|C_n|$ where $|C_n|$ is the duration of C_n . In the case of discrete time, a sum-term of the form $\sum_k g(z_k)$ replaces the integral. We do not specify how to determine the control cycles C_n , and they can have an a-priori constant length, or their termination can be the result of certain events.

For example, let the plant consist of an M/D/1 queue, u_n is the value of the service time during C_n , and y_n is the time-average of the sojourn times of all jobs arriving during C_n . IPA can be used to compute the derivative $\frac{\partial y_n}{\partial u_n}$ via a well-known formula [3]. Generalizing this example, suppose that the plant-system is a stochastic event-driven system (DEDS or HS), $u \in R$ is a control variable, assumed to have a constant value (u_n) during C_n , $y_n \in R$, is a random function of u_n as indicated by Eq. (2), and its derivative $L'_n(u_n)$ is computed by IPA. Later we will be concerned with measurement and computational errors and hence modify Eqs. (2) and (3) accordingly.

The development of the proposed regulation technique has been motivated primarily by applications to computer cores, especially regarding regulation of power and instruction-throughput by adjusting the core's clock rate (frequency) [5], [6]. Concerning throughput, there are no prescriptive, let alone analytic models for the frequency-to-throughput relationship, and a complicated, intractable queueing model has had to be used for simulation. Nonetheless a simple IPA algorithm has been developed and used to approximate the sample derivative for determining the integrator's gain via Eq. (3). The regulation technique was extensively tested on programs from an industry-based suite of benchmarks, Splash-2 [7], using a detailed simulation platform for performance assessment of computer architectures, Manifold [8]. We reported the results in [2], [6], [9], and deemed them encouraging and meriting a further exploration of the regulation technique.

In the context of IPA research, this regulation technique represents two new perspectives. First, the traditional application of IPA throughout its development has been to optimization, whereas here it is applied in a new way, namely to performance regulation. Second, much of the research of IPA has focused on its unbiasedness, whereas here, in contrast, the concern is with fast computation which may come at the expense of accuracy and unbiasedness. The main novelty of the paper as compared to References [2], [6], [9] is in the fact that it concerns not simulation but an actual implementation. In this we were facing new challenges associated with real-time measurements, computations, and control. Consequently we were unable to control each core separately as in [2], [6], [9], and hence applied the regulation

method to a processor containing multiple cores. Furthermore, due to issues with real-time computation, we were forced to take drastically cruder approximations to the IPA derivatives than in [2], [6], [9], and in fact it seems that we drove the degree of imprecision to the limit. How this worked on application programs will be seen in the sequel. In any event, the work described here is, to our knowledge, the first implementation (beyond simulation) of IPA in a real-time control environment.

The rest of the paper is structured as follows. Section 2 summarizes relevant convergence results of the regulation technique in an abstract setting. Section 3 describes the system under study and its model, presents simulation results on Manifold followed by implementation on a state-of-the-art computer processor, and compares the two. Section 4 derives some lessons from these results and proposes directions for future research.

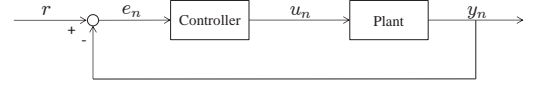


Fig. 1. Abstract regulation system

II. CONVERGENCE RESULTS

This section recounts established results concerning convergence of the regulation technique defined by recursive applications of Eqs. (1) to (4), as summarized in Ref. [2]. Ideally convergence means that

$$\lim_{n \rightarrow \infty} e_n = 0, \quad (5)$$

hence $y_n \rightarrow r$ (see Figure 1). This can be achieved under suitable assumptions (mentioned below) if the plant system is time invariant, and hence the function $L(u) = L_n(u)$ does not depend on $n = 1, \dots$. In that case the control loop comprised of Equations (1)-(4) essentially implements Newton's method for solving the equation $r - L(u) = 0$, for which there are well-known sufficient conditions for convergence. These include situations where the derivative term $L'(u_n)$ in Eq. (3) is computed in error, for which convergence in the sense of (5) is ascertained under upper bounds on the magnitude of the error [10].

If the system is time varying, Eq. (5) may not hold true, and in this case convergence can be characterized by the equation

$$\limsup_{n \rightarrow \infty} |e_n| < \varepsilon, \quad (6)$$

where $\varepsilon > 0$ depends on a measure of the system's variability. To make matters concrete let $J : R \rightarrow R$ be a differentiable function, and suppose that the term $y_n := L_n(u_n)$ in Eq. (2) is a functional approximation of $J(u_n)$. Assuming that $L_n(\cdot)$ is differentiable as well, we can view the term $L'_n(u_n)$ as an approximation to $J'(u_n)$ in (3). However, for reasons that will be seen in the sequel, we add another layer of approximation to $L'_n(u_n)$, denoted by ζ_n , so that Eq. (3) computes the term

$L'_n(u_n) + \zeta_n$. Defining $\psi_n := L_n(u_n) - J(u_n)$ and $\phi_n = L'_n(u_n) + \zeta_n - J'(u_n)$, Eqs. (2) and (3) become

$$y_n = L_n(u_n) = J(u_n) + \psi_n, \quad (7)$$

and

$$A_{n+1} = \left(L'_n(u_n) + \zeta_n \right)^{-1} = \left(J'(u_n) + \phi_n \right)^{-1}, \quad (8)$$

respectively. The regulation technique now is defined by recursive applications of Eqs. (1),(7),(8),(4).

To analyze its convergence, suppose first, to simplify the discussion, that there exists a closed, finite-length interval, I , such that every point u_n computed by the regulation algorithm is contained in I ; this assumption will be removed later. Moreover, I satisfies the following assumption.

Assumption 1: (i) The function J and the functions L_n are differentiable throughout I . (ii) The function J is either convex or concave, and monotone increasing or decreasing throughout I . (iii) There exists $u \in I$ such that $J(u) = 0$.

Various ways to relax this assumption will be discussed shortly. The following result was proved in [2].

Proposition 2.3 and Lemma 2.2 in [2]: For every $\varepsilon > 0$, $\eta > 0$, and $M > 1$, there exist $\alpha \in (0, 1)$, $\delta > 0$, and $\theta \in (0, 1)$ such that, for every interval I satisfying Assumption 1 and the following two additional conditions: (i) $\eta \leq \min\{|J'(u)| : u \in I\}$, and (ii) $\max\{|J'(u)| : u \in I\} \leq M \min\{|J'(u)| : u \in I\}$:

1). If for some $j \in \{1, 2, \dots\}$, and for $n = j, j+1, j+2$, $u_n \in I$, $|\phi_n| \leq \alpha|J'(u_n)|$, and $|\psi_n| \leq \delta$, then

$$|e_j| < \theta|e_{j-2}|. \quad (9)$$

2). If for all $n = 1, 2, \dots$, $u_n \in I$, $|\phi_n| \leq \alpha|J'(u_n)|$, and $|\psi_n| \leq \delta$, then

$$\limsup_{n \rightarrow \infty} |e_n| < \varepsilon. \quad (10)$$

□

In the context of the system considered in this paper, what we have in mind is a situation where the plant is an event-driven system controlled by a real-valued parameter u , $J(u)$ is an expected-value function defined over a finite horizon (hence not in steady state and possibly dependent on an initial condition), $y_n = L_n(u_n) + \psi_n$ is a sample-based approximation (possibly biased!) of $J(u_n)$ over the control cycle C_n , and $L'_n(u) + \phi_n$ is a sample approximation of $J'(u_n)$.

A few remarks concerning Assumption 1 are due.

1). The differentiability assumption is unnecessary, convexity of $J(u)$ and almost-sure differentiability of $L_n(u)$ at a given point u suffice. These conditions often arise in the context of IPA. Under these weaker assumptions the proofs in [2] can be carried out in the context of convex analysis rather than differentiable calculus.

2). The condition that $u_n \in I$, $n = 1, \dots$, can be enforced in the case where I is a constraint set for the sequence $\{u_n\}$. In that case Eq. (1) would be replaced by

$$u_n = P_I(u_{n-1} + A_n e_{n-1}) \quad (11)$$

where $P_I(v)$ is the projection of $v \in R$ onto I , i.e., the point in I closest to v . The proof of convergence is unchanged.

3). Often the magnitude of the error terms ψ_n and ϕ_n can be controlled by taking longer control cycles, but there is no way to ensure the inequalities $|\phi_n| \leq \alpha|J'(u_n)|$ and $|\psi_n| \leq \delta$ for every $n = 1, 2, \dots$, which is stipulated as a condition for Eq. (10). Practically, however, with long-enough control cycles we can expect those inequalities to hold for finite strings of $n \in \{k_1, \dots, k_2\}$, thus guaranteeing the validity of Eq. (9). If these strings are long enough, Equation (9) would result in e_n approaching 0 at a geometric rate, then periodically jumping away due to the sporadic occurrence of larger errors, but again returning towards 0 rapidly, etc. This behavior has been observed in all of the examples where we tested the regulation technique for a variety of event-driven systems [2], [6], [9], [11].

4). Another source of the jitters described in the previous paragraph is the time-varying nature of the system. This is particularly pronounced in the system tested in this paper, since the workload of programs processed by a core can vary widely in unpredictable ways. Nonetheless we shall see that the regulation algorithm gives good results.

5). It is possible to ascertain the assumptions underscoring the analysis in [2] for simple systems (e.g., tandem queues and some marked graphs), but may be impossible to ascertain them for more complicated systems. For instance, it can be impossible to prove differentiability or even convexity of an expected-value function from characterizations of its sample realizations, or bounds on the errors associated with IPA. Moreover, some of these assumptions, including convexity or concavity, were made in [2] in order to enable an analysis but may not be necessary. The aforementioned convergence results serve to explain the behavior of the regulation method that was observed in all of our former experiments [2], [6], [9], [11] as well as in those described later in this paper.

III. MODELING, SIMULATION, AND IMPLEMENTATION

The system-architecture considered in this paper is based on an Out-of-Order (OOO) core technology whereby instructions may complete execution in an order different from the program order, hence the “out of order” designation. This enables instructions’ execution to be limited primarily by data dependency and not by the order in which they appear in the program. Data dependency arises when an instruction requires variables that first must be computed by other instructions. A detailed description of OOO architectures can be found in [12], while a high-level description is contained in [2]. Here we provide an abstract functional and logical description, and refer the reader to [2] for a more-detailed exposition.

The functionality of an OOO core is depicted in Figure 2.¹ Instructions are fetched sequentially from memory and placed in the instruction queue, where they are processed by functional units, or servers in the parlance of queueing theory. The queue is assumed to have unlimited storage and

¹Typically a core is dedicated to the processing of a program or a thread, namely a subprogram, as determined by the programmer or the operating system. In the forthcoming discussion we will use the term *program* to designate a thread as well.

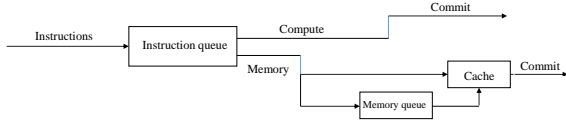


Fig. 2. High-level instruction flow in OOO architectures

there is a server associated with each buffer. The processing of an instruction starts as soon as it arrives *and* all of its required variables become available. The instruction departs from the queue as soon as its execution is complete *and* the previous instruction (according to the program order) departs. In the parlance of computer architectures, an instruction is said to be *committed* when it departs from the queue. The instruction-throughput of the core is defined and measured by the average number of instructions committed per second.

Instructions generally are classified as *computational instructions* or *memory instructions*. Access times of external, off-chip, memory instructions are one-to-two orders of magnitude longer than those of computational instructions. Therefore most architectures make use of a hierarchical memory arrangement where on-chip cache access takes less time than external memory such as DRAM. First the cache is searched, and if the variable is found there then it is fetched and the instruction is completed. If the variable is not stored in cache (a situation known as *cache miss*) then it is fetched from external memory (typically DRAM) and placed in the cache, whence it is accessed and the instruction is completed. External memory instructions can be thought of as being placed in a finite-buffer, first-in-first-out queue, designated as the *memory queue* in Figure 2. When this queue becomes full, the entire memory access, including cache, is stalled. Thus, there are three causes for an instruction to be stalled: a computational or memory instruction waiting for variables computed by other instructions, a memory instruction waiting for the memory queue to become non-full, and any instruction waiting (after processing) for the previous instruction to depart from the queue. We point out that instructions involving computation and L_1 cache-access are subjected to the core's clock rate, while memory instructions involving external memory, such as DRAM, are not subjected to the same clock. This complicates the application of IPA and may cause it to be biased.

A quantified discrete-event model of this process is presented in the appendix, and a more general description can be found in [2], which also contains a detailed algorithm for the IPA derivative of the throughput as a function of frequency.

A. Manifold Simulation

We use a cycle-level, full system discrete event simulation platform for multi-core architectures, Manifold. The simulated model consists of a 16-core X86 processor die, where each core is in a separate clock domain and can control its own clock rate independently of other cores. For a detailed description of the Manifold simulation environment and its capabilities, please see Ref. [8].

We simulated two application programs from the benchmark-suite Splash-2, Barnes and Water-ns [7]. Barnes is a computation-intensive, memory-light application while Water-ns is memory intensive. For each execution, all of the 16 cores of the processor run threads of the same benchmark concurrently while each one of them is controlled separately. The control cycle is set to 0.1 ms for both Barnes and Water-ns. The frequency range of the cores is set to $[0.5GHz, 5.0GHz]$. We assume a continuous frequency range for the simulations, but later will consider a realistic, discrete range for the implementation described in the sequel. The target instruction throughput is set to the same value for each core for both Barnes and Water-ns, and we experiment with the target throughput values of 1,200 MIPS (Million Instructions per Second), 1,000 MIPS, and 800 MIPS. In terms of instructions per control cycle, these target values correspond to 0.12×10^6 , 0.1×10^6 , and 0.08×10^6 , respectively. The relationship between clock frequency and instruction throughput is determined by the Manifold processor model, but its IPA derivative was computed according to the high-level instruction flow described above and in the appendix. For each application run we present, in the following paragraphs, the results for one of the 16 cores chosen at random.

Consider first the target throughput of 1,200 MIPS. The throughput simulation results for the Barnes benchmark are shown in Figure 3, where the horizontal axis indicates time in ms and the vertical axis indicates instruction throughput. We discern a rise of the throughput from its initial value (measured at 643.1 MIPS) towards the target level of 1,200 MIPS, which it reaches for the first time in about 1.5 ms, or 15 control cycles. Thereafter it oscillates about the target value, which is not surprising due to the unpredictable, rapidly-changing program workload. The average throughput computed over the time interval $[1.5ms, 100ms]$ (soon after the throughput has reached the target value) is 1,157.4 MIPS, which is 42.6 MIPS off the target level of 1,200 MIPS.

Figure 4 depicts the graph of frequency vs. time (in ms), and it shows some saturation at its highest level of 5.0 Ghz, in the time-interval $[7ms, 12ms]$. Saturation at the highest level can correspond to a negative offset of the average throughput from its target level, since it indicates that the system may be unable to raise the throughput to a desired level. During the period of frequency saturation indicated in Figure 4, the throughput shown in Figure 3 it more jittery and sporadically attains slightly-lower values than after time 25ms. It also shows these characteristics between the end of the saturation period and time 25ms. Therefore, the extent of the effects of the saturation on the aforementioned offset of 46.4 MIPS is not clear. Nonetheless we mention this point since it will be more pronounced in some of the results on which we report later. Also, we computed the average throughput in the intervals $[30ms, 100ms]$ and $[50ms, 100ms]$, after the jittery behavior of the throughput has somewhat subsided. The results are 1,192.6 MIPS and 1,192.9 MIPS, respectively, corresponding to offsets of 7.4 MIPS and 7.1 MIPS from the target throughput of 1,200 MIPS. These

results suggest that the frequency saturation plays some role in the larger, 46.4-MIPS offset that was computed over the interval $[1.5ms, 100ms]$.

For the target throughput of 1,000 MIPS, the results (not shown due to space limitations) showed a rise in throughput from its initial value of 420.5 MIPS to 1,000 MIPS in 2.1 ms, or 21 control cycles. The average throughput in the $[2.1ms, 100ms]$ interval is 990.2 MIPS, corresponding to an offset of 9.8 MIPS of the throughput from its target value of 1,000 MIPS. The frequency saturated at its upper limit only at 5 isolated control cycles with minimal effects on the throughput.

For the throughput target of 800 MIPS, the results show a rise in the throughput from its initial value of 679.3 MIPS to 800 MIPS in 1.9 ms, or 19 iterations. The average throughput in the interval $[1.9ms, 100ms]$ was 839.6 MIPS, which is 39.6 MIPS off the target value of 800 MIPS. There was a considerable frequency saturation at the lowest level of 0.5 GHz, which explains the positive offset.

Returning to the results for the target level of 1,200 MIPS, we considered a way to reduce the throughput oscillations and frequency saturation by scaling down the gain in Eq. (1). We did this by replacing Eq. (1) by the following equation,

$$u_n = u_{n-1} + \xi A_n e_{n-1}, \quad (12)$$

for a suitably-chosen constant $\xi \in (0, 1)$. After some experimentation on various benchmarks (excluding those tested here) we chose $\xi = 0.2$. The resulting frequencies did not saturate throughout the program's run, and yielded an average throughput of 1,198.5 MIPS, which is 1.5 MIPS off the target level of 1,200 MIPS. Though working well for this example, this technique may be problematic when used with an implementation rather than simulation, as will be discussed in the next subsection.

For Water-ns, consider first the throughput target of 1,200 MIPS. Simulation results of throughput and frequency are shown in Figure 5 and Figure 6, respectively. We notice greater fluctuations and more saturation than for Barnes. In particular, Figure 6 shows three distinct periods of frequency saturations at its upper limit of 5.0 GHz, and Figure 5 shows very low throughput during these periods. To explain this, recall that Water-ns is a memory-heavy program, and execution times of memory instructions are longer (typically by one or two orders of magnitude) than computational instructions. During those periods the instructions of Water-ns mainly concern memory access, which are low-throughput instructions. The controller is applying its highest frequency in order to push the throughput to its target value, but that frequency is not high enough to have much effect. This is why the periods of high-limit frequency saturation are characterized by very low throughput. This has a pronounced affect of lowering the average frequency measured during the program's execution. In fact, the throughput obtained from the simulation rises from its initial value of 429 to its target level of 1,200 MIPS in about 1.8 ms, or 18 control cycles (this rise is not evident from Figure 5 due to its insufficient granularity), and the average throughput from the time the

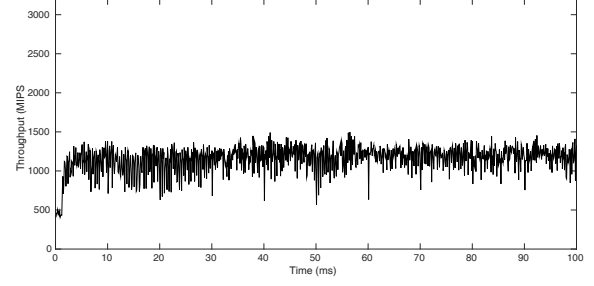


Fig. 3. Manifold simulation, Barnes: throughput vs. time, target = 1,200 MIPS

TABLE I
MANIFOLD SIMULATIONS: OFFSET OF AVERAGE THROUGHPUT FROM
TARGET LEVELS

Target Throughput (MIPS)	1,200	1,000	800
Barnes	-42.6	-9.8	39.6
Water-ns	-73.2	-52.2	62.6

target level is reached (1.8ms) to the end of the program-run (333ms) is 1,126.8 MIPS, which is 73.2 MIPS off the target level of 1,200 MIPS. Despite this offset, we observe that as soon as the program transitions from memory mode to computational mode, as indicated by the end of the saturation periods in Figure 6, the throughput returns quickly to about its target level, as can be seen in Figure 5.

For the target throughput of 1,000 MIPS, simulation results show the throughput increasing from its initial value of 472.1 MIPS to the target level on 1,000 MIPS in 2.3 ms, or 23 control cycles. There is considerable frequency saturation at the high limit of 5.0 GHz. The average throughput in the interval $[2.3ms, 330ms]$ is 947.8 MIPS, which means an offset of 52.2 MIPS off the target throughput.

For the target throughput of 800 MIPS, simulation results indicated a rise of the throughput from its initial value of 443.3 to its target level in about 2.3 ms, or 23 control cycles. There is considerable saturation of the frequency at its lower level of 0.5 GHz, and hence a positive offset between the computed average throughput and its target level. Indeed, the average throughput in the interval $[2.3ms, 330ms]$ is 862.6, MIPS, hence meaning an offset of 62.6 MIPS of the throughput from its target value of 800 MIPS.

All of these results are summarized in Table I, showing the offset (in MIPS) of average throughput from target throughput, obtained from Manifold simulations of Barnes and Water-ns with throughput targets of 1,200, 1,00, and 800 MIPS.

Returning to the throughput target of 1,200 MIPS, an application of the modified algorithm with $\xi = 0.2$ in Eq. (12) yielded the average throughput of 1,143.6 MIPS which is 56.4 MIPS off the target level of 1,200 MIPS. This is a smaller offset than the 73.2 MIPS obtained from the unmodified algorithm, and it is explained by the fact that there is still considerable, though less frequency saturation than with the unmodified algorithm.

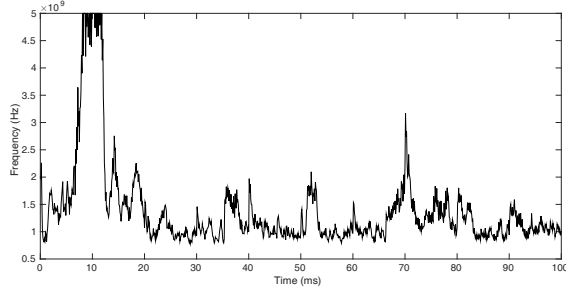


Fig. 4. Manifold simulation, Barnes: clock frequency vs. time, target = 1,200 MIPS

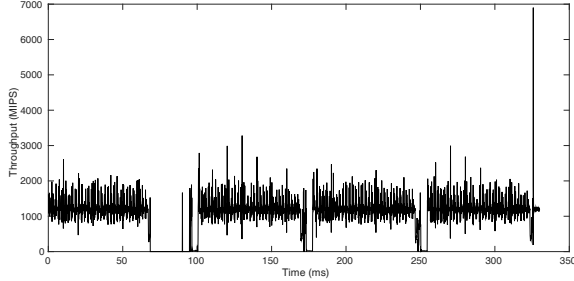


Fig. 5. Manifold simulation, Water-ns: throughput vs. time, target = 1,200 MIPS

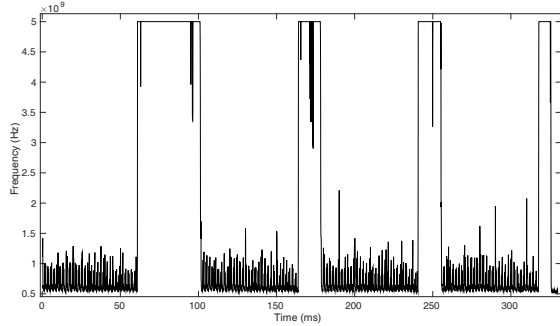


Fig. 6. Manifold simulation, Water-ns: clock frequency vs. time, target = 1,200 MIPS

B. Haswell implementation

Haswell is Intel's fourth-generation core processor architecture fabricated in the 22nm process [13]. Haswell is comprised of multiple out-of-order execution cores designed for improved power efficiency over prior generations. The version used in our study has four cores residing on each Haswell processor. Each core supports two threads. All the cores execute at the same frequency, the *processor frequency*.

Since the four cores operate at the same frequency, we cannot control each core separately by the frequency. Instead, we consider the average throughput among the active threads, which we call the *normalized processor throughput*, or *normalized throughput* in brief; it is the equivalent measure of the core's frequency in the Manifold model described above. We point out that typically the programmer and operating system distribute the load among the various cores in a

balanced way, and in the system considered here there are 4 cores executing 8 threads, two threads to a core.

We implemented the controller by loading a C++ program to the processor via the PAPI interface [14].² Recall that the control algorithm is based on Eqs. (1),(2),(8),(4). However, the Haswell processor admits only a finite set of 16 frequencies, and we have to modify Eq. (1) accordingly. This set of frequencies, denoted by Ω , is (in GHz) $\Omega = \{0.8, 1.0, 1.1, 1.3, 1.5, 1.7, 1.8, 2.0, 2.2, 2.4, 2.5, 2.7, 2.9, 3.1, 3.2, 3.4\}$. Denoting by $[u]$ the nearest point to $u \in \mathbb{R}$ in the set Ω (the left point in case of a tie), we modify Eq. (1) by Eq. (13), below. The control algorithm is formalized as follows.

Notation: C_n - the n th control cycle; r - the target normalized throughput; u_n - the processor frequency during C_n ; y_n - the resulting measured normalized throughput; $e_n := r - y_n$.

Algorithm 1: The following steps are taken during C_n :

- 1) At the start of C_n , set

$$u_n = [u_{n-1} + A_n e_{n-1}]. \quad (13)$$

- 2) During C_n , measure y_n , and compute an approximation to the IPA derivative, $\frac{\partial y_n}{\partial u_n}$, denoted by $\tilde{\lambda}_n$; note that $\tilde{\lambda}_n = \frac{\partial y_n}{\partial u_n} + \zeta_n = L'_n(u_n) + \zeta_n$ in Eq. (8).
- 3) At the end of C_n , set $A_{n+1} = (\tilde{\lambda}_n)^{-1}$.
- 4) At the end of C_n , compute $e_n := r - y_n$.

The IPA algorithm used for the Manifold simulation is too complicated for a real-time implementation, and therefore we explored approximations thereto with the objective of having them be as simple as possible. The simplest we could find was

$$\tilde{\lambda}_n = \frac{y_n}{u_n}, \quad (14)$$

and we argue for that on the following grounds. The frequency-to-throughput performance function $y_n := L_n(u_n)$ is monotone increasing and has a linear component. As a matter of fact, if there are no external-memory instructions then the throughput is linear in the core's frequency, as can be seen from the analysis in the appendix and in [2]. In that case $\tilde{\lambda}_n = \frac{\partial y_n}{\partial u_n}$. With a mix of memory and computing instructions, the function $L_n(u_n)$ can be thought of as having a linear component (with a time-varying slope) and a nonlinear component. We expect the error term $\tilde{\lambda}_n - \frac{\partial y_n}{\partial u_n}$ to be larger, and consequently the regulation technique to work less well, for intensive memory programs like Water-ns than for memory-light programs like Barnes. This is evident from the testing we performed, whose results are presented in the following paragraphs.

²Modern microprocessors include many hardware counters that record the occurrences of various events during program executions. Examples of such events include i) completion of the execution of an integer instruction, ii) a cache miss, or iii) an instruction that accesses memory. The Performance Application Programming Interface (PAPI) is a publicly available software infrastructure for accessing these performance counters during program execution.

Consider first the results obtained from the testing of Barnes. For the throughput target of 1,200 MIPS, the results are shown in Figure 7, where the horizontal axis indicates time in ms and the vertical axis indicates instruction throughput. The total run time is 100 ms, and it corresponds to about 1,000 control cycles. The throughput rises from an initial value of 739.2 MIPS to the target level of 1,200 MIPS in about 1.3 ms, or 13 control cycles. The average throughput computed over the time interval $[1.3\text{ms}, 100\text{ms}]$ (soon after the throughput has reached the target value) is 1,166.5 MIPS, which is 33.5 MIPS off the target level of 1,200 MIPS. The graph of the frequencies is shown in Figure 8, and it indicates no saturation throughout the program. We partly attribute the 33.5-gap to the quantization error due to the rounding off of the frequencies to their nearest values in Ω , which is evident from Figure 8.

For the target level of 1,000 MIPS, the throughput climbed from its initial value of 633.2 MIPS to its target level in 1.5 ms, or 15 control cycles. There was no frequency saturation, and the average throughput in the $[1.5\text{ms}, 330\text{ms}]$ interval is 990.6, which means an offset of 9.4 MIPS from the target level of 1,000 MIPS.

For the target level of 800 MIPS, the throughput climbs from its initial value of 763.1 to the target level in 1.0 ms, or 10 control cycles. There was no frequency saturation, and the average throughput is 829.7 MIPS, which is 29.7 MIPS off the target level of 800 MIPS. Again, we attribute this gap to the saturation error.

Recall that we proposed a way to reduce the throughput oscillations and frequency saturation by modifying the control algorithm, by replacing Eq. (1) by Eq. (12) with $\xi = 0.2$. Although this worked well for the Manifold simulation with the throughput target of 1,200 MIPS, it yielded poor results for the Haswell implementation. After a few iterations the processor frequency was “stuck” at a value and did not move away from it. The reason is in the quantization error inherent in the algorithm, which is due to the rounding off of the computed control variable in Eq. (13). The step size for modifying the control variable is insufficient to take that variable out of its current value.

Regarding Water-ns, results for the throughput target of 1,200 MIPS are shown in Figure 9. The throughput rises from an initial value of 683.1 MIPS to its target value of 1,200 MIPS in about 2.1 ms, or 21 control cycles. The throughput oscillates at its upper level more than that obtained for Barnes, and this is due to the fact that Water-ns is a memory-heavy application. For the same reason, there is considerable frequency saturation throughout the program as indicated in Figure 10. The obtained average throughput in the interval $[2.1\text{ms}, 333\text{ms}]$ is 1143.2 MIPS, which is 56.8 MIPS off the target level of 1,200 MIPS.

For the throughput level of 1,000 MIPS, the throughput rises from its initial value of 780 MIPS to its target level in 2.5 ms, or 25 control cycles. While there is some frequency saturation at the upper limit of the frequency range, the average throughput is 1,014.4 MIPS, which is 14.4 MIPS off its target level.

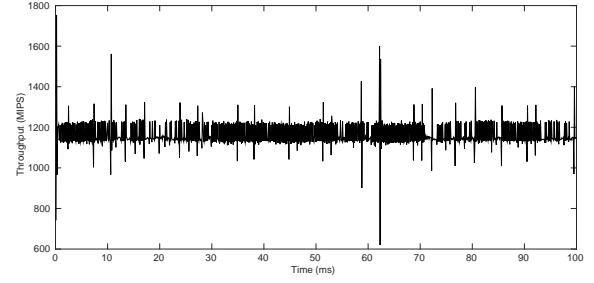


Fig. 7. Haswell implementation, Barnes: throughput vs. time, target = 1,200 MIPS

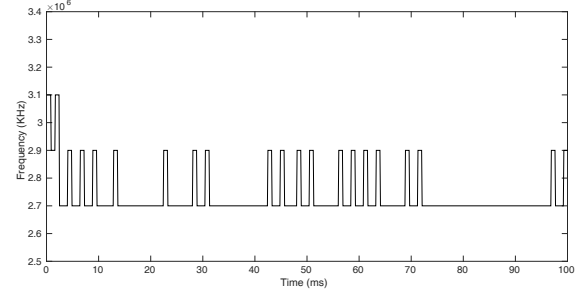


Fig. 8. Haswell implementation, Barnes: clock frequency vs. time, target = 1,200 MIPS

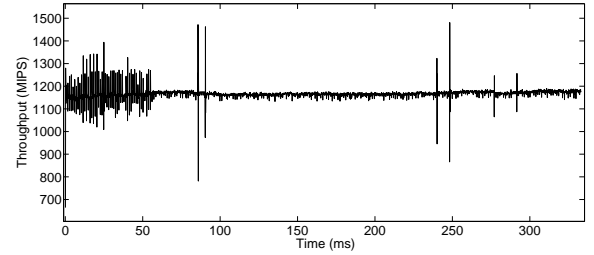


Fig. 9. Haswell implementation, Water-ns: throughput vs. time, target = 1,200 MIPS

Finally, for the target throughput of 800 MIPS, the throughput rises from its initial value of 698.3 to its target level in 2.4 ms, or 24 control cycles. There are considerable frequency oscillations at the upper limit of the frequency range, and the average throughput is 836.3, which is 36.3 MIPS off the target level.

These results are summarized in Table II, showing the offset (in MIPS) of average throughput from target throughput, obtained from Haswell implementation of Barnes and Water-ns with throughput targets of 1,200, 1,000, and 800 MIPS.

Comparing the data summarized in Table I and Table II, we see that the regulation technique performs slightly better on the Haswell implementation platform than on the Manifold

TABLE II

Target Throughput (MIPS)	1,200	1,000	800
Barnes	-33.5	-9.4	29.7
Water-ns	-56.8	14.4	36.3

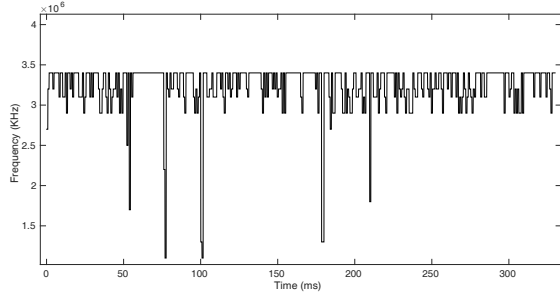


Fig. 10. Haswell implementation, Barnes: clock frequency vs. time, target = 1,200 MIPS

simulation environment. The reason for this may be due to the fact that in the simulation experiment we regulate the throughput of each core separately, while in the implementation we control the average throughput of all the cores in the processor.

IV. CONCLUSIONS

This paper describes the testing of an IPA-based throughput regulation technique in multicore processors. The testing was performed on both a simulation environment and an implementation platform. Despite crude approximations that have had to be made in the implementation setting, the proposed technique performed slightly better than in the simulation setting. Future research will extend the regulation method from a centralized control of a single processor to a distributed control of networked systems.

V. APPENDIX

This section provides a quantitative description of the instruction-flow in the OOO-cache high-level model described at the beginning of Section III.

Denote by I_i , $i = 1, 2, \dots$, the instructions arriving at the instruction queue in increasing order. Let u denote the clock rate, or frequency, and let $\tau := u^{-1}$ be the clock cycle. Denote by $a_i(\tau)$ the arrival time of I_i relative to the arrival time of I_1 , namely $a_1(0) := 0$, and let ξ_i be the clock counter at which I_i arrives. Then, $a_i(\tau) = \xi_i \tau$. Denote by $\alpha_i(\tau)$ the time at which execution of I_i starts, and let $\beta_i(\tau)$ denote the time at which execution of I_i ends.

We next describe a way to compute $\alpha_i(\tau)$. consider first the case where I_i is a computational instruction. If all of its required variables are available at its arrival time then $\alpha_i(\tau) = a_i(\tau) + \tau$. On the other hand, if I_i has to wait for such variables, let $k(i)$ denote the index (counter) of the instruction last to provide such a variable, then $\alpha_i(\tau) = \beta_{k(i)}(\tau) + \tau$. Next, if I_i is a memory instruction, then $\alpha_i(\tau)$ is the time it starts a cache access. If the memory queue is not full at time $a_i(\tau)$, then $\alpha_i(\tau) = a_i(\tau) + \tau$. On the other hand, if the memory queue is full at time $a_i(\tau)$, let $\ell(i)$ denote the index of the instruction at the head of the queue, then, $\alpha_i(\tau) = \beta_{\ell(i)}(\tau) + \tau$.

To compute $\beta_i(\tau)$, consider first the case where I_i is a computational instruction. Let μ_i denote the number of clock

cycles it takes to execute I_i . Then, $\beta_i(\tau) = \alpha_i(\tau) + \mu_i(\tau)$. On the other hand, if I_i is a memory instruction, let v_i denote the number of clock cycles it takes to perform a cache attempt. If the cache attempt is successful and the variable is found in cache, then $\beta_i(\tau) = \alpha_i(\tau) + v_i(\tau)$. If the variable is not in cache, the instruction is directed to the memory queue. Its transfer there involves a small number of clock cycles, m_i , hence it arrives at the queue at time $\alpha_i(\tau) + v_i\tau + m_i\tau$. The memory queue is a FIFO queue whose service time represents an external-memory access, which is independent of the core's clock. Denote by S_i the sojourn time of I_i at the memory queue. Then $\beta_i(\tau) = \alpha_i(\tau) + v_i\tau + m_i\tau + S_i + \tau$.

Finally, the departure time of I_i from the instruction queue, denoted by $d_i(\tau)$, is $d_i(\tau) = \max\{\beta_i(\tau), d_{i-1}(\tau)\} + \tau$. Given a control cycle consisting of N instructions, the throughput is defined as $N/d_N(\tau)$. Since $u = \tau^{-1}$, we can view the throughput as a function of u and denote it by $y(u)$. Its IPA derivative, $\frac{\partial y}{\partial u}$, can be computed by following the above dynamics of the instructions' flow. This, and a more detailed discussion of the model, can be found in [2].

REFERENCES

- [1] G.F. Franklin, J.D. Powell, and A. Emami-Naeini, *Feedback Control of Dynamic Systems*, Prentice Hall, 2015.
- [2] Y. Wardi, X. C. Seatzu, Chen, and S. Yalamanchili, Performance Regulation of Event-Driven Dynamical Systems Using Infinitesimal Perturbation Analysis, under review in *Nonlinear Analysis: Hybrid Systems*, also in Arxiv, Ref. arXiv:1601.03799v1 [math.OC], 2016.
- [3] Y.C. Ho and X.R. Cao, *Perturbation Analysis of Discrete Event Dynamic Systems*, Kluwer Academic Publishers, Boston, Massachusetts, 1991.
- [4] C. Cassandras and S. LaFortune, *Introduction to Discrete Event Systems*, Kluwer Academic Publishers, Boston, Massachusetts, 1999.
- [5] N. Almoosa, W. Song, Y. Wardi, and S. Yalamanchili, A Power Capping Controller for Multicore Processors, *Proc. 2012 American Control Conference*, Montreal, Canada, June 27-29, 2012.
- [6] N. Almoosa, W. Song, Y. Wardi, and S. Yalamanchili, Throughput Regulation in Multicore Processors via IPA, *Proc. 51 IEEE Conference on Decision and Control (CDC)*, Maui, Hawaii, December 10-13, 2012.
- [7] S.C. Woo, M. Oharat, E. Torriet, J. Singhi and A. Gupta, The SPLASH-2 Programs: Characterization and Methodological Considerations, *Proceedings of the ISCA 22nd Annual International Symposium on Computer Architectures (ISCA95)*, Santa Margherita Ligure, Italy, 1995.
- [8] J. Wang, J. Beu, R. Behda, T. Conte, Z. Dong, C. Kersey, M. Rasquinha, G. Riley, W. Song, H. Xiao, P. Xu, and S. Yalamanchili, Manifold: A Parallel Simulation Framework for Multicore Systems, *Proc. IEEE International Symposium on Performance Evaluation of Systems and Software (ISPASS)*, 2014.
- [9] X. Chen, H. Xiao, Y. Wardi, and S. Yalamanchili, Throughput Regulation in Shared Memory Multicore Processors, *Proc. 22nd IEEE Intl. Conference on High Performance Computing (HiPC)*, Bengaluru, India, December 16-19, 2015.
- [10] P. Lancaster, Error analysis for the Newton-Raphson method, *Numerische Mathematik*, Vol. 9, pp. 55-68, 1966.
- [11] C. Seatzu, and Y. Wardi, Performance Regulation via Integral Control in a Class of Stochastic Discrete Event Dynamic Systems, *Proc. 12th IFAC - IEEE International Workshop on Discrete Event Systems (WODES'14)*, Paris, France, May 14-16, 2014.
- [12] J.L. Hennessey and D.A. Patterson, *Computer Architecture: A Quantitative Approach*, Morgan Kaufmann, 2012.
- [13] P. Hammarlund and et al, Haswell: The Fourth-Generation Intel Core Processor, *Micro*, pp. 6 - 20, 2014.
- [14] S. Browne, J. Dongarra, N. Garner, G. Ho, and P. Mucci, A Portable Programming Interface for Performance Evaluation on Modern Processors, *The International Journal of High Performance Computing Applications*, Volume 14, number 3, pp. 189-204, Fall 2000.